BJRS

BRAZILIAN JOURNAL
OF
RADIATION SCIENCES
11-03 (2023) | 01-12 | e2281

New Deformity Outline on the Breast Radiation Therapy for diminishing Absorbed Dose Ratio

Khorshidi[a], A.; Ashoor[a], M.

[a] *Radiation Application Research School, Nuclear Science and Technology Research Institute, Tehran, Iran*

e-mail address of the corresponding author: abkhorshidi@yahoo.com

ABSTRACT

Breast cancer is one of the most common malignant diseases in women. After tumor mass surgery, radiation therapy is regularly taken into account the gold standard for the treatment. Kilo to Mega voltage photons have been suggested due to their characteristic depth dose build-up regime, reducing the dose to the breast skin to a fraction of the maximum dose exposure. During treatment, mean glandular dose is commonly used as a criterion for identifying radiation risks. Here, two outlines in cubic-rectangular (CR) and cylindrical- taper (CT) outlines were modelled together with corresponding assumptions using Monte-Carlo simulation and the recorded absorbed dose ratio (ADR) values were compared via defined a positron source by 511 keV energy. The results showed that the amounts of absorption and scattering cross-sections next to the ADR amount decreased as the height of the CR outline decreased. The average dose ratio amount in the CR outline was reduced by about 96% compared to that in the CT outline. By increasing the positron source distance from the nipple, the ADR amounts decreased for both outlines. The amount of accumulated dose ratio decreased harshly in the CR outline rather than in the CT outline. This study can be useful to examine breast tissue deformity in treatment planning.

Keywords: **Positron radiation, Breast cancer; Deformity; Absorbed Dose ratio.**

ISSN: 2319-0612
DOI: https://doi.org/10.15392/2319-0612.2023.2281
Submitted: 2023-05-10
Accepted: 2023-06-20

1. INTRODUCTION

The analyses of the breast tumor and tissue by the mammography system and also its treatment play a central role since ionizing radiation is used. As known, the female breast consists mainly of ducts, lobules and stroma, as shown in Figure 1a. Hormones are of great importance in many cases of the corresponding cancer; except how it happens is not completely understood. A common symptom of breast cancer is a new lump or mass on a regular basis. Painless, hard mass with irregular boundaries is likely more cancerous that can be easily ruptured or tendered. Other possible breast cancer disorders include: swelling, irritation of the skin or dimpling, pain in the nipple or breast tissue, redness, scaliness, thickening of the skin or nipple, nipple retraction and discharge [1,2]. The mammary glands consist of a large series of lobular ducts lined with epithelium capable of secreting milk. These ducts empty into larger milk-carrying ducts that converge at the nipple. These glandular constructions are implanted in backing fatty tissue, and the breasts are divided into lobules by connective tissue. The majority of breast cancers start in the cells lining the ducts and some in the lobules, while a small number start in other tissues. The ductal carcinoma in situ is frequently reflected to be pre-invasive or non-invasive breast cancer [3,4]. In treatment, the average glandular dose is used as a criterion for identifying the radiation risk. This dose is evaluated assuming the equivalent homogeneous tissue [5,6]. In reality, the accuracy of this estimation is controversy because that is inhomogeneous. Here in this survey, the amount of absorbed dose ratio (ADR) for the dissimilar breast outlines such as CR and CT shapes is examined along with the corresponding assumptions to decrease the absorbed dose in the normal tissues by the Monte-Carlo simulations.

Figure 1. *a) The cylindrical-taper (CT) outlook of the breast organ (top).*
b) Diagram of the breast as cubic-rectangular (bottom-left) and CT (bottom-right) outlines.

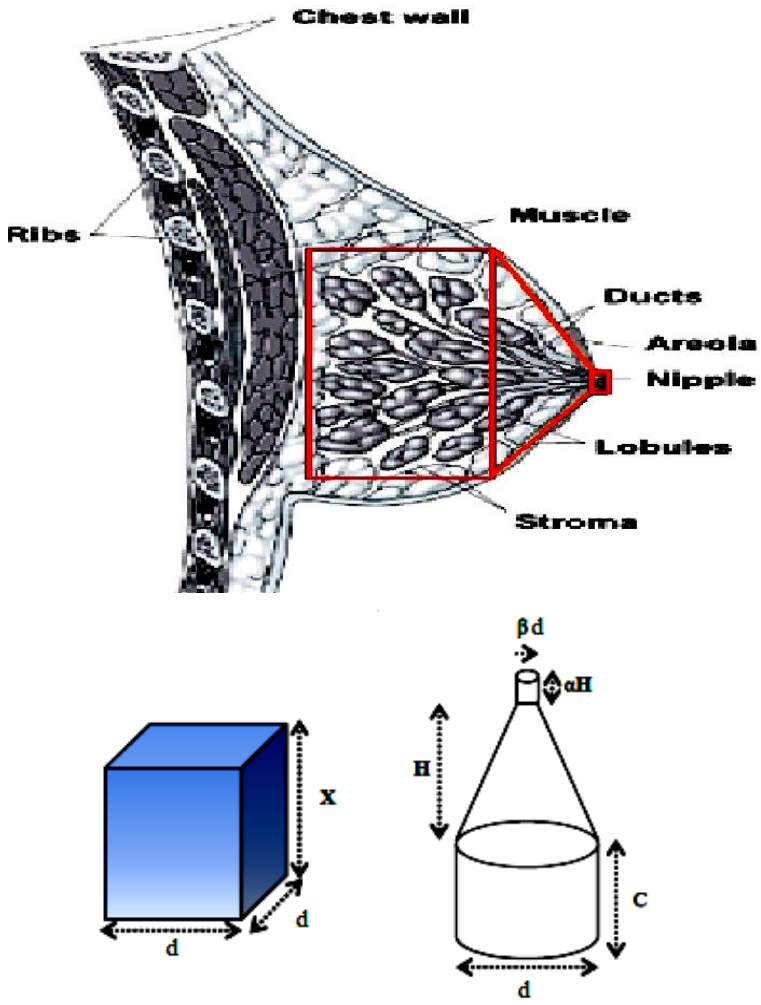

2. MATERIALS AND METHODS

The breast cancer can be examined through mammography images. If the cancer is detected at early stages, it can be properly treated by radiation [7-9]. The goal of mammography is to detect cancers before it causes symptoms. The breast cancer is discovered because it tends to get noticeably larger and is more likely to have previously spread beyond the breast. Also in treatment, by virtue of radiation propagating in the materials, there is an interaction that results in the amount of energy being put into them that is valuable for tumor and not normal tissue. In order to decrease the ADR as well

as increase the efficiency and signal-to-noise (SNR) ratio, the processes are proposed based on *breast tissue deformity* and *shielding strategy* problems. One of these is the geometric variations in breast configuration during imaging and/or treatment. Here, the dissimilar outlines of the breast are defined as CT and CR, as shown in Figure 1b. The volumes of these forms (V_{CT} and V_{CR}) are similar and equal to the constant value since the density of the breast is invariant under all deformation conditions. To satisfy this assumption, one can get the connection between parameters of dissimilar geometric outlines (CT and CR) as follows,

$$V_{CT} = d^2 \times X \quad \text{(Equation 1)}$$

$$V_{CR} = \pi \frac{d^2}{4} \times C + \frac{1}{3}\pi \frac{d^2}{4} \times H + \pi \left(\frac{\beta d}{2}\right)^2 \times \alpha H \quad \text{(Equation 2)}$$

Here, it equates the two expressions, and it can be calculated for X and K:

$$\pi \frac{d^2}{4} \times C + \frac{1}{3}\pi \frac{d^2}{4} \times H + \pi \left(\frac{\beta d}{2}\right)^2 \times \alpha H = d^2 \times X \quad \text{(Equation 3)}$$

$$\pi \frac{1}{4} \times C + \frac{1}{3}\pi \frac{1}{4} \times H + \pi \left(\frac{\beta}{2}\right)^2 \times \alpha H = X \quad \text{(Equation 4)}$$

$$\pi \left[\frac{1}{4} \times C + \frac{1}{12}\pi \times H + \pi \left(\frac{\beta}{2}\right)^2 \times \alpha H\right] = X$$

$$X = \pi \left[\frac{(1+3\alpha\beta^2)H}{12} + \frac{C}{4}\right] \quad \text{(Equation 5)}$$

$$K = C + (1+\alpha)H \quad \text{(Equation 6)}$$

where β and α are the trivial fractional numbers of cylinder diameter (d) and cone height (H), correspondingly. The X and K amounts are the height of the CR sketch and the total height of the CT sketch, respectively. Eqs. 5 and 6 are independent of the d value. Here, the base of the breast does not have a main role in the calculations. Schematically, these equations are drawn in Figure 2 at values of K = 20, 15, and 10 cm when the β and α values approach to zero. The decreasing ratio of X with increasing H is determined in theory as a slope of -0.5235 representing an angle of 152.5°, which is entitled deformity angle of the outlined breast. The changing ratio of X against H has a constant amount under all situations. The scattering and absorption cross sections decreased with the X reduction in the CR sketch, and concomitantly the ADR decreased.

Figure 2. *The cube length of X versus cone height of H, a) with the nipple width for K = 20 cm and α = 0.1, b) the sum of the cone heights for K = 10, 15, and 20 cm while α and β values come near to zero.*

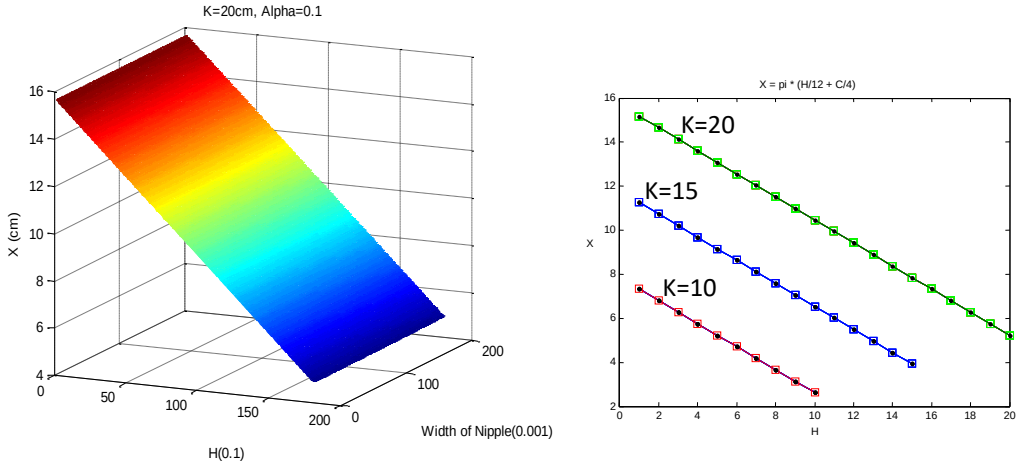

The Monte Carlo N-Particles code version X (MCNP-X) [10] is modified to obtain a history from the contributions of each of the positrons towards producing the ADR. This code is very applicable due to accessible and more controllable on all parameters included in computations and tractable particle detections based on the different nuclear cross sections as well as having potential estimate of the flux, dose and Kerma [10,11]. The library that was here utilized for MCNPX simulations was ENDF/B-VII.0 [12]. The breast volume was in the range of 400 to 1500 cm^3 [13].

The amount of positron source energy is 511 keV as mono-energetic and propagated to the front and end of the breast. The equivalent tissue density is defined by 104E-2 g/cm^3. For CR shape, 12×12×6.55 cm^3 geometrical dimensions were outlined. On the other hand, the CT outline is as a small cylinder (D = 1.2 cm, H = 1 cm), a cone (D = 12 cm, H = 10 cm), and a large cylinder (D = 12 cm, C = 5 cm). Also, the source was located at distances of 0.5 and 15.5 cm from the nipple on the right breast away from the heart to reduce possible risks to the heart. For the simulation, the trajectories of 1E+7 photons were calculated using the workstation of F4 tally and cards of dose function and energy by Q-factor of 1, and the mean error was estimated.

3. RESULTS AND DISCUSSION

The alterations of the CR height versus the cone height of CT outline and the size of breast nipple have been shown in Figure 2a, for K = 20 cm and α = 0.1. When the cone height enlarged, the CR height reduced meaningfully at a distinct slope, that is, the minimum deformity occurs while the part of the cone part at the CT outline is unimportant rather than that of the cylinder. Subsequently, the sizeable breasts have the smallest height for the CT outline, and then the most dose amount is absorbed rather than the CR outline. The cube height (X) as a function of cone height (H) whereas the entire cone height is at a distinct value at α = β = 0 is indicated in Figure 2b (unit in terms of cm). While the nipple size is negligible, there is a constant slope, namely the deformity angle. However, with the variation of this size, the angle is varied. Subsequently, whilst the tumor is located in the nipple, the calculations are deviated as trivial. The CR, CT, and CT-CR outlines were simulated by MCNPX code, as shown in Figure 3. The ADR value decreased in CT outline at 0.5 cm distance of the nipple due to increasing depth and decreasing the number of particles as a function of depth.

Figure 3. *The modelled breast deformity via MCNPX simulator, a) cubic- rectangular (CR), b) cylindrical-taper (CT), c) CR and CT outlines.*

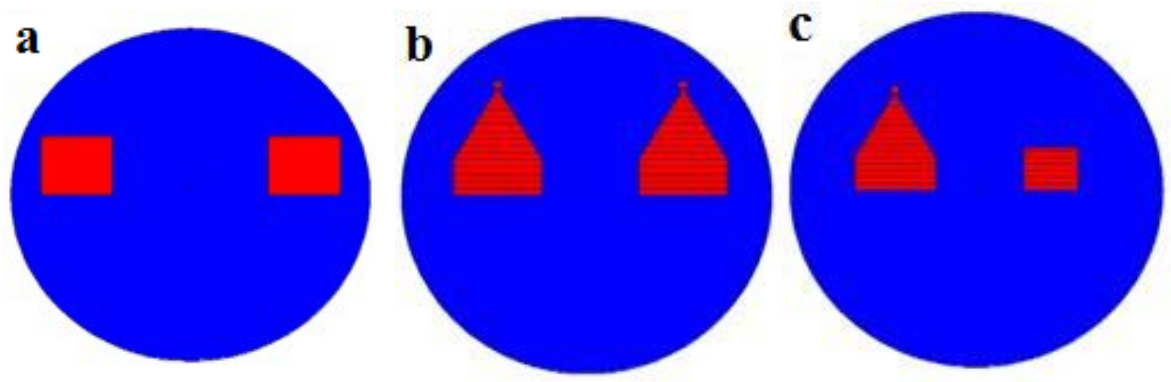

The ADR amounts are different in CT outline in both left and right breasts. While the positron source is close to the right breast, the ADR value at the right barest (RB) is more than that of the left breast (LB) for the reason that the attenuation value was increasing with the increase in distance from

the source and depth, according to Figure 4. The relative difference between absorbed dose ratio (ADR) as the depth function is also demonstrated for the LB and RB in CT outline. This disparity is raised in the lesser depths and reduced with the increase of depth as exponential function by 22E-3 MeV/(g.cm) gradient and moved towards zero more than 18 cm depth.

Figure 4. *The simulated absorbed dose ratio as a function of the depth in the left and right breasts (LB and RB) for CT (top) and CR (bottom) outlines at Z distances of 0.5 and 15.5 cm of the nipple (left). The relative difference at ADRs in the RB and LB for CT and CR outlines (right).*

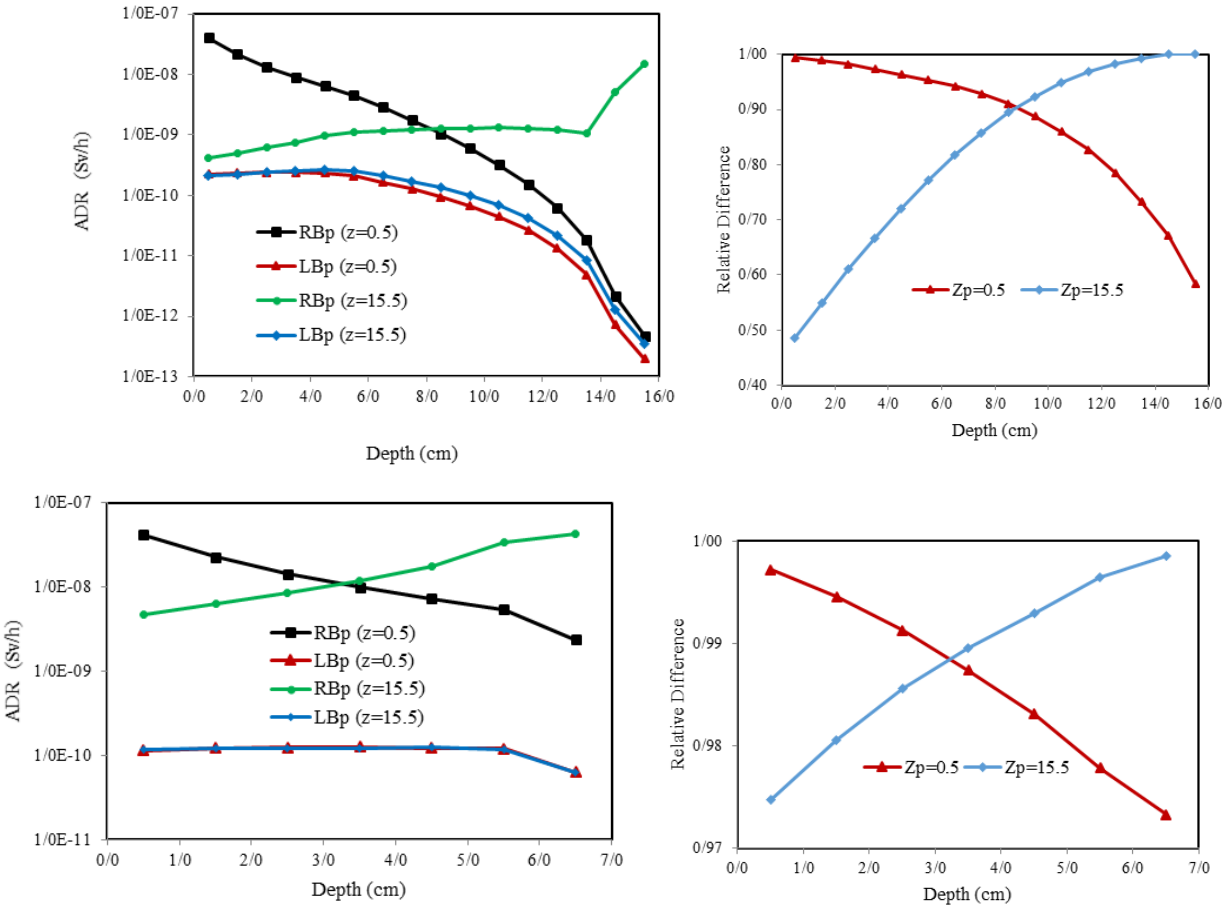

The ADR values in both left and right breasts also were different in CR outline of deformed breast. While the positron source was close to the right breast, the ADR value was more independent of the defined depth rather than CT outline, and the differences between them were unimportant by raising the depth, as shown in Figure 4. The relative difference amounts between the ADRs for the LB and

RB in CR outline as the depth function is also demonstrated. Again, this disparity was elevated in the lower depths, and decreased by increasing the depth in the form of a linear function by 5E-3 MeV/(g.cm) slope.

Table 1 indicates the pileup ADRs in the RB and LB of CT and CR outline at distances of 0.5 and 15.5 cm from the nipple, respectively. At these distances, these accumulated ADRs in CT outline were 98% and 95% more than that of CR outline, respectively. As a result, the normal breast should be located in the CR outline for treatment planning, as there is a high likelihood of the formation of tumors in the nipple.

Table 1. Accumulated dose ratio (Sv/h) by Q-factor of 1 at LB-CR and RB-CT outlines.

Source location from right breast (cm)	Cube (Deformed LB)	Taper (RB)	Difference
15.5 cm	1.633E-09	3.432E-08	95.24%
0.5 cm	1.616E-09	1.022E-07	98.42%

When planning treatment, one can take into account the amount of absorbed dose into the other tissues. There are generally many factors that influence the qualification of images as well as absorbed radiation dose, one of which is the scattered rays. These rays cab be attenuated by the grids. Inaccuracies in grids design and breast geometry configuration design lead to an increase in absorbed dose in the breast due to their flexibility. Recently, Buonanno et al. [14] have demonstrated a possibility of utilizing low energy X-ray spectra rotationally by 150 kV that the dose distribution in phantom revealed a skin-to-tumor dose ration of 34% for a dedicated lesion at 5.25 cm from cylinder axis in comparison to megavoltage radiotherapy.

The simulated ADR value at 511 keV in CT outline decreased locally with increasing the depth as the energy of the rays decreased. At dissimilar depths, the ADR values were approximately constant in the CR rather than the CT, but the probability of interaction enlarged in the CT outline by virtue of large solid angle. The smaller the solid angle, the lower the likelihood of interactions, so the ADR amount decreased because the generation and interaction of rays followed a random model.

Here, the total error in dose calculations was less than 5%. While some abnormal tissues are irradiated, the others inevitably absorb the dose of scattered rays. For instance, the nontarget and

adjacent tissues absorb an average of 14.3% of the dose in the breast [15,16]. However, due to the statistical oversights and variability, there was a slight discrepancy between the reported and the calculated amounts [17,18]. The deformity angle presented in Eq. (5) is a firm principle and does not alter under different conditions. There is a small error in the results as the breast cannot be precisely traced by the CR outline due to the curvature of the edges and boundaries.

In general, although x-ray and gamma sources are used for treatment and diagnosis [19-22], positron sources are primarily used to diagnose diseases [23-27]. Therefore, in this research, positron energy was utilized for treatment procedures. In future researches, the energies of combined sources can be used to achieve higher and better treatment estimates.

4. CONCLUSIONS

In this investigation, a new technique was proposed based on the breast deformity in order to diminish the dose in nearby normal tissues. This deformation on the breast is possible in the CR outline due to the greater flexibility. The results revealed that at the low energy of the positron source, these amounts diminished by increasing the depth, depending on the source position. The ADR amounts at disparate depths were almost constant in the CR outline rather than the CT, but the likelihood of interactions increased in the CT outline due to the large solid angle of deformity. The lower the solid angle, the lower the interaction probability becomes, so the ADR amount diminished because the generation and interaction of rays involves a random model. In summary, deforming breast geometry can help avoid of further damages in treatment and imaging problems.

REFERENCES

[1] Joe, B. N.; Lee, A. Y. **Breast Imaging**, E-Book: The Core Requisites. Elsevier Health Sciences, 2022.

[2] Gershenson, D. M.; Lentz, G. M.; Valea, F. A.; Lobo, R. A. **Comprehensive Gynecology**. Elsevier Health Sciences, 2021.

[3] Winters, S.; Martin, C.; Murphy, D.; Shokar. N. K. Breast Cancer Epidemiology, Prevention, and Screening. **Progress in Molecular Biology and Translational Science,** v. 151, p. 1-32, 2017. https://doi.org/10.1016/bs.pmbts.2017.07.002

[4] Feng, Y. et al. Breast cancer development and progression: Risk factors, cancer stem cells, signaling pathways, genomics, and molecular pathogenesis. **Genes & Diseases,** v. 5, p. 77-106, 2018. https://doi.org/10.1016/j.gendis.2018.05.001

[5] Oscar, A.; Villarreal, M.; Velasco, F. G.; Fausto, A. M. F.; Mas Milian, F.; Mol, A. W.; Capizzi, K. R.; Ambrosio, P. Optimization of the exposure parameters in digital mammography for diverse glandularities using the contrast-detail metric. **Physica Medica,** v. 101, p. 112-119, 2022. https://doi.org/10.1016/j.ejmp.2022.08.009

[6] Fitton, I.; Noël, A.; Minassian, J.; Zerhouni, M.; Wojak, J.; Adel, M.; Fournier, L. Technical note: Design and initial evaluation of a novel physical breast phantom to monitor image quality in digital breast tomosynthesis. **Medical Physics**, v. 49, p. 2355-2365, 2022. https://doi.org/10.1002/mp.15498

[7] Maqsood, S.; Damaševičius, R.; Maskeliūnas, R. TTCNN: A Breast Cancer Detection and Classification towards Computer-Aided Diagnosis Using Digital Mammography in Early Stages. **Applied Sciences**, v. 12, p. 3273, 2022. https://doi.org/10.3390/app12073273

[8] Altameem, A.; Mahanty, C.; Poonia, R. C.; Saudagar, A. K. J.; Kumar, R. Breast Cancer Detection in Mammography Images Using Deep Convolutional Neural Networks and Fuzzy Ensemble Modeling Techniques. **Diagnostics**, 12, p. 1812, 2022. https://doi.org/10.3390/diagnostics12081812

[9] Balleyguier, C.; Cousin, M.; Dunant, A.; Attard, M.; Delaloge, S.; Arfi-Rouche, J. Patient-assisted compression helps for image quality reduction dose and improves patient experience in mammography. **European Journal of Cancer**, v. 103, p. 137-142, 2018. https://doi.org/10.1016/j.ejca.2018.08.009

[10] Pelowitz, D. B. editor. **MCNPX user's manual version 2.6.0, LA-CP-07-1473.** New Mexico, United States: Los Alamos National Laboratory (LANL), 2008.

[11] Authors on behalf of ICRP, Eckerman, K.; Harrison, J.; Menzel H. G.; Clement C. H. **ICRP Publication 119: Compendium of Dose Coefficients based on ICRP Publication 60**. Ann ICRP, v. 42, p. e1-e130, 2013. doi: 10.1016/j.icrp.2013.05.003

[12] **Evaluated Nuclear Data File**; 2009. Available at: https://www-nds.iaea.org/public/download-endf/ENDF-B-VII.0/. Last accessed: 2009 -01-18.

[13] Velden, B. H. M.; Vos, B. D.; Loo, C. E.; Kuijf, H. J.; Isgum, I.; Gilhuijs, K. G. A. Response monitoring of breast cancer on DCE-MRI using convolutional neural network-generated seed points and constrained volume growing. **Proc SPIE 10950, Medical Imaging 2019: Computer-Aided Diagnosis, 109500D,** 13 March 2019. doi: 10.1117/12.2508358

[14] Buonanno, F.; Sarno, A.; De Lucia, P. A.; Di Lillo, F.; Masi, M.; Di Franco, F.; Mettivier, G.; Russo, P. Rotational radiotherapy of breast cancer with polyenergetic kilovoltage X-ray beams: An experimental and Monte Carlo phantom study. **Physica Medica**, v. 62, p. 63-72, 2019. doi: 10.1016/j.ejmp.2019.05.002

[15] Svahn, T. M.; Houssami, N.; Sechopoulos, I.; Mattsson, S. Review of radiation dose estimates in digital breast tomosynthesis relative to those in two-view full-field digital mammography. **Breast,** v. 24, p. 93-9, 2015 doi: 10.1016/j.breast.2014.12.002

[16] Maajani, K.; Jalali, A.; Alipour, S.; Khodadost, M.; Tohidinik, H. R.; Yazdani, K. The Global and Regional Survival Rate of Women with Breast Cancer: A Systematic Review and Meta-analysis. **Clin Breast Cancer**, v. 19, p. 165-177, 2019. doi: 10.1016/j.clbc.2019.01.006

[17] Nakamura, T.; Suzuki, S.; Takei, Y.; Kobayashi, I.; Pongnapang, N.; Kato, K. Simultaneous measurement of patient dose and distribution of indoor scattered radiation during digital breast tomosynthesis. **Radiography**, v. 25, p. 72-76, 2019. doi: 10.1016/j.radi.2018.10.006

[18] Choi, J. S.; Rim, C. H.; Kim, Y. B.; Yang, D. S. Cumulative radiation exposure dose of diagnostic imaging studies in breast cancer patients. **Inte J Radiat Res**, v. 17, p. 275-281, 2019. doi: 10.18869/acadpub.ijrr.17.2.275

[19] Khorshidi, A. Accelerator driven neutron source design via beryllium target and 208Pb moderator for boron neutron capture therapy in alternative treatment strategy by Monte Carlo method. **Journal of Cancer Research and Therapeutics**, v. 13, p. 456-465, 2017. doi: 10.4103/0973-1482.179180.

[20] Khorshidi, A. Nano Yttrium-90 and Rhenium-188 production through medium medical cyclotron and research reactor for therapeutic usages: A Simulation study. **Nuclear Engineering and Technology**, v. 55, p. 1871-1877, 2023. doi: 10.1016/j.net.2023.02.013

[21] Khorshidi, A. Segmentation of tumor region in respiratory disease by extended algorithm. **International Journal of Modern Physics C**, 2023; In Press. doi: 10.1142/S0129183123501644

[22] Khorshidi, A. Assessment of SPECT images using UHRFB and other low-energy collimators in brain study by Hoffman phantom and manufactured defects. **The European Physical Journal Plus**, v. 135, p. 261, 2020. doi: 10.1140/epjp/s13360-020-00238-6

[23] Souza, G. C. de A.; Gontijo, R. M. G.; Silva, J. B. da; Mamede, M.; Ferreira, A. V. Spatial resolution of a preclinical PET tomograph. **Brazilian Journal of Radiation Sciences**, v. 9(1A), 2021. https://doi.org/10.15392/bjrs.v9i1A.1503

[24] Bispo, A. C. de A.; Nascimento, L. T. C. do; Castro, A. C. F.; Lima, L. A. R.; Ferreira, S. M. Z. M. D.; Silva, J. B. da; Mamede, M. Synthesis and characterization of the radiopharmaceutical [18F]fluoroestradiol. **Brazilian Journal of Radiation Sciences**, v. 9(1A), 2021. https://doi.org/10.15392/bjrs.v9i1A.1387

[25] Paiva, F. G.; Santana, P. C.; Mourão Filho, A. P. Patient dose reduction by changing the amount of 18F-FDG radiopharmaceutical injected. **Brazilian Journal of Radiation Sciences**, v. 7(2A (Suppl.), 2019. https://doi.org/10.15392/bjrs.v7i2A.704

[26] Pessanha, P. R.; de Queiroz Filho, P. P.; Santos, D. de S. Dosimetric evaluation of extremities in 18F-FDG PET/CT procedure using Monte Carlo Geant4 code. **Brazilian Journal of Radiation Sciences**, v. 7(3B (Suppl.), 2019. https://doi.org/10.15392/bjrs.v7i3B.890

[27] Santana de Souza, S. A.; Monteiro Rodrigues, F.; Fattori Alves, A. F.; Alvarez, M.; Molena Seraphim, D.; Lopes Ruiz Junior, R.; Souza Trindade Filho, J. C.; Marrone Ribeiro, S.; Pina, D. R. Quality and Quantity Assessment of Tomographic Exams That Can Be Performed on Existing Hybrid Equipment at Botucatu Medical School Nuclear Medicine Services. **Brazilian Journal of Radiation Sciences**, v. 10(2), 2022. https://doi.org/10.15392/bjrs.v10i2.1799.